# The XENON10 WIMP Direct Detection Search at the Gran Sasso Underground Laboratory

Aaron Manalaysay[1]

*Department of Physics, University of Florida, Gainesville, FL 32611, USA*
*Physics Institute, University of Zürich, Zürich, CH-8057, Switzerland*

**Abstract.** The direct detection search for WIMPs with the XENON10 detector has produced among the best results in the field to date. The detector is a dual-phase liquid xenon time projection chamber, capable of 3-D position reconstruction and nuclear recoil discrimination. We summarize 58.6 live-days of WIMP search data collected at the Gran Sasso Underground Laboratory (LNGS) in Italy. With this data we have been able to set stringent upper limits on the spin-dependent and spin-independent WIMP scattering cross sections, in addition to a lower limit of 2.2 TeV/$c^2$ on the mass of the heavy Majorana neutrino.

**Keywords:** xenon, direct detection
**PACS:** 95.35.+d,29.40.Mc,95.55.Vj

## INTRODUCTION

The XENON10 experiment searches for evidence of elastic collisions between Weakly Interacting Massive Particles (WIMPs) and xenon nuclei. Such particles, which have been proposed as a possible dark matter candidate, arise naturally in a number of theories beyond the Standard Model [1, 2]. A large non-relativistic relic population of WIMPs could exist today that was produced via the generic mechanism of thermal freeze-out in the early Universe.

By construction, WIMPs participate in weak interactions and hence should scatter with quarks and leptons. Scattering events in terrestrial particle detectors by WIMPs with mass in the range 10 GeV/$c^2$ to 100 TeV/$c^2$ would be primarily manifested as nuclear recoils below 100 keV, assuming they exist in an approximately smooth, isothermal halo around the Milky Way. Many technologies have been employed, and proposed, to search for this type of signature [3, 4].

Liquid xenon (LXe) embodies a number of properties deemed useful in a WIMP direct detection experiment. For low recoil energies (below $\sim$30 keV), the cross section for spin-independent WIMP-nucleus interactions scales with $A^2$, and thus LXe searches benefit from xenon's $\sim$130 nucleons, which comprise one of the largest nuclei suitable for particle detection. Additionally, roughly half of naturally occurring xenon nuclei have spin ($^{129}$Xe and $^{131}$Xe) making it a suitable choice for spin-dependent WIMP-nucleus scattering searches as well. The dominant background in any current WIMP search comes from gamma rays. Xenon's high $Z$ means it acts as a formidable shield of

[1] Presented on behalf of the XENON collaboration. Electronic mail: aaronm@physik.uzh.ch

CP1166, *Sources and Detection of Dark Matter and Dark Energy in the Universe*,
edited by D. B. Cline

such backgrounds, with the outer layers of a xenon detector blocking many background gamma rays from reaching inner layers. This phenomenon, known as 'self shielding', cannot combat backgrounds originating from the detector medium itself, but fortunately there exist no long-lived xenon radioisotopes. Finally, when used under certain conditions (described in the next section) LXe permits the distinction between nuclear recoils and electronic recoils on an event-by-event basis.

## THE XENON10 DETECTOR

The XENON10 detector is a 3-D position sensitive dual phase (liquid-gas) xenon Time Projection Chamber (TPC). The active volume is 20 cm in diameter and 15 cm in height, defined on the perimeter by a hollow polytetrafluoroethylene (PTFE) cylinder and on top and bottom by grid electrodes. The cathode grid electrode at the bottom and the gate grid at the top define a downward electric field of 0.73 kV/cm; 5 mm above the gate grid is the anode grid, with the liquid level lying between the gate and anode. A fourth grid, 5 mm above the anode, is held at the same potential as the gate grid, and serves to prevent any extracted electrons from escaping the anode. After fiducial cuts, the mass of LXe used for the WIMP search is 5.4 kg.

Ionizing radiation produces prompt scintillation and ionization in xenon [5]. While some of the ionization electrons recombine at the interaction site and contribute to the direct scintillation signal, the electric field produced by the grid electrodes on top and bottom drifts the remaining electrons up to the liquid surface and into the gas where they produce proportional scintillation as they accelerate onto the anode grid electrode. In this way both prompt scintillation ('S1') and ionzation ('S2') signals can be measured simultaneously with photomultiplier tubes (PMTs). The fraction of ionization electrons that recombine depends on the incoming particle species, with electronic recoils exhibiting characteristically weaker electron recombination than nuclear recoils. Because of this, the ratio of S2 to S1 can be used to distinguish between the two types of recoils. This last feature, called nuclear recoil discrimination, is able to remove on an event-by-event basis upwards of 99.9% of the remaining gamma backgrounds that reach the inner regions of the detector, and is a vital component of any WIMP search. The signal window is broken up into seven bins; in each bin, the cut efficiencies, nuclear recoil acceptance, nuclear recoil discrimination power, number of total observed events, and expected number of events in the signal region are shown in Table 1.

Fig 1 (left) shows characteristic PMT output traces from a scattering gamma ray (electronic recoil) and a scattering neutron (nuclear recoil). The S1 signals are nearly identical at roughly 70 photoelectrons (p.e.) each, while the S2 signal of the electronic recoil is clearly larger, giving a larger value of the ratio S2/S1. This ratio is shown quantitatively as a function of energy in Fig 1 (right) for a gamma calibration with $^{137}$Cs and a neutron calibration with AmBe. These sources were used to calibrate the position of the bands only; in order to calibrate the electronic recoil energy scale a $^{57}$Co source was used, which provides a 122 keV gamma ray. The nuclear recoil energy can be found from the relation, $E_{nr} = E_{er}/\mathscr{L}_{eff} \times S_e/S_n$, where $E_{er}$ is the electronic recoil energy based on the $^{57}$Co scale, $\mathscr{L}_{eff}$ is the relative scintillation efficiency of nuclear recoils taken to be 0.19 in this energy range, and $S_{e(n)}$ is the quenching factor of electronic

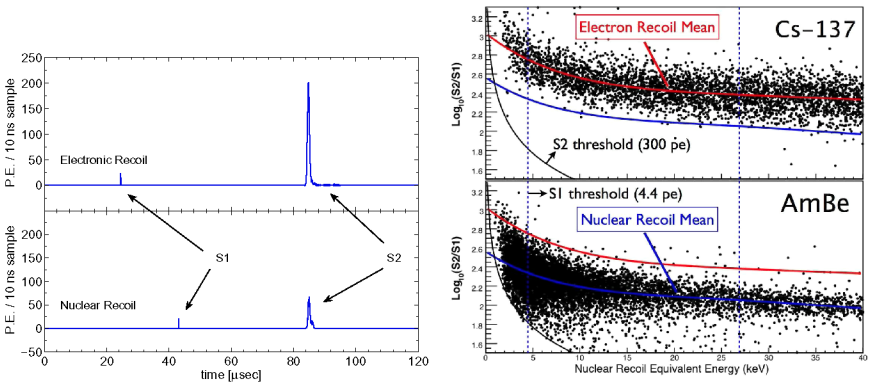


**FIGURE 1.** (*Left*) Traces from gamma and neutron recoils. The S1 signals for both traces are equal, while the S2 signal of the gamma recoil is much larger. The ratio S2/S1 is used to distinguish between electronic and nuclear recoils. (*Right*) The bands formed in $\log_{10}$(S2/S1) vs. S1 space for (top) electronic recoils from $^{137}$Cs and (bottom) nuclear recoils from AmBe.

**TABLE 1.** The software cut acceptance of nuclear recoils $\varepsilon_c$, the nuclear recoil acceptance $A_{nr}$, and the electron recoil rejection efficiency $R_{er}$ for each of the seven energy bins ($E_{nr}$ in nuclear recoil equivalent energy). The expected number of leakage events, $N_{leak}$, is based on $R_{er}$ and the number of detected events, $N_{evt}$, in each energy bin, for the 58.6 live-days WIMP-search data, with 5.4 kg fiducial. Errors are the statistical uncertainty from the Gaussian fits on the electron recoil $\Delta\log_{10}(S2/S1)$ distribution.

| $E_{nr}$ (keV) | $\varepsilon_c$ | $A_{nr}$ | 1 - $R_{er}$ ($10^{-3}$) | $N_{evt}$ | $N_{leak}$ |
|---|---|---|---|---|---|
| 4.5 - 6.7 | 0.94 | 0.45 | $0.8^{+0.7}_{-0.4}$ | 213 | $0.2^{+0.2}_{-0.1}$ |
| 6.7 - 9.0 | 0.90 | 0.46 | $1.7^{+1.6}_{-0.9}$ | 195 | $0.3^{+0.3}_{-0.2}$ |
| 9.0 - 11.2 | 0.89 | 0.46 | $1.1^{+0.9}_{-0.5}$ | 183 | $0.2^{+0.2}_{-0.1}$ |
| 11.2 - 13.4 | 0.85 | 0.44 | $4.1^{+3.6}_{-2.0}$ | 190 | $0.8^{+0.7}_{-0.4}$ |
| 13.4 - 17.9 | 0.83 | 0.49 | $4.2^{+1.8}_{-1.3}$ | 332 | $1.4^{+0.6}_{-0.4}$ |
| 17.9 - 22.4 | 0.80 | 0.47 | $4.3^{+1.7}_{-1.2}$ | 328 | $1.4^{+0.5}_{-0.4}$ |
| 22.4 - 26.9 | 0.77 | 0.45 | $7.2^{+2.4}_{-1.9}$ | 374 | $2.7^{+0.9}_{-0.7}$ |
| Total | | | | 1815 | $7.0^{+1.4}_{-1.0}$ |

(nuclear) recoils due to the applied electric field measured to be 0.54 (0.93) at 0.73 kV/cm [6]. Using the AmBe neutron calibration, a comparison between data and Monte Carlo has been performed to estimate both the ionization and scintillation efficiencies in this energy range [7]. Once the electronic and nuclear recoil bands are defined by the data shown in Fig 1 (right), we define the WIMP search window, not in terms of $\log_{10}$(S2/S1), but in terms of the distance from the electronic recoil band centroid, $\Delta\log_{10}$(S2/S1).

## WIMP SEARCH RESULTS

The WIMP search results reported here comprise 58.6 live-days of background data collected at the Gran Sasso Underground Laboratory (LNGS) between October 6, 2006 and February 14, 2007. LNGS provides approximately 3100 m water equivalent of rock overburden as shielding against atmospheric muons. The WIMP search was performed blind, meaning that the energy window and all cuts were defined beforehand based on calibration data and existing non-blind background data. The signal acceptance region is defined to lie between 4.5 and 26.9 keV recoil equivalent (keVr), and between $\mu$ and $\mu - 3\sigma$ where $\mu$ and $\sigma$ are the estimators of the mean and standard deviation of the nuclear recoil band in $\Delta\log_{10}$(S2/S1) space, based on a Gaussian fit to the AmBe calibration data. The data, along with this acceptance window, are shown in Fig 2. The ten events in the signal region, shown as the circled data points, are consistent with background.

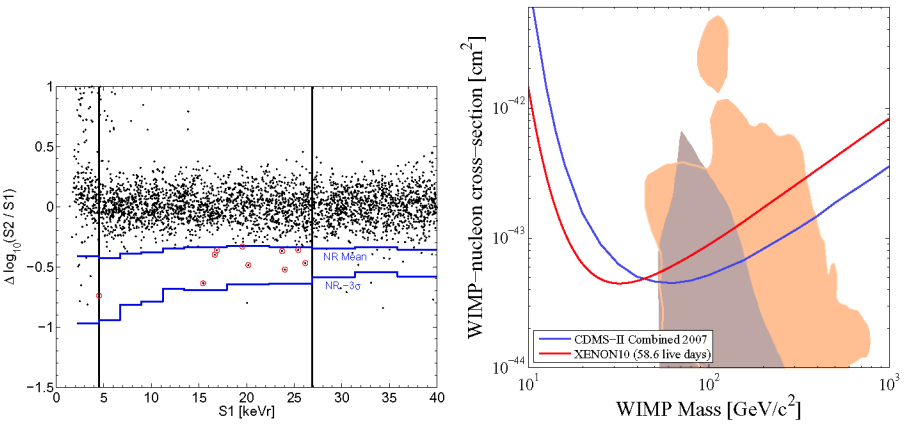


**FIGURE 2.** (*Left*) Results from a blind analysis of 58.6 live days. The energy window is defined by the two vertical lines. The vertical acceptance region is defined to lie between $\mu$ and $\mu - 3\sigma$ of the nuclear recoil band, indicated by the horizontal steps in the figure. The horizontal scale is given as 'keVr' which means keV in the nuclear recoil energy scale. (*Right*) Upper limits on the spin-independent WIMP-nucleon cross section. Also shown are the most recent limits from CDMS-II [8] and from theoretically favored regions from CMSSM [9, 10].

To set limits on WIMP interaction cross sections, we treat the blind WIMP search data using the Yellin Maximum Gap method [11], considering all ten events in the signal region without background subtraction. The upper limits on the WIMP interaction cross sections are calculated assuming a standard set of halo parameters, described in [1, 12]. As the interaction between WIMPs and quarks may have contributions from scalar (spin-independent) and axial vector (spin-dependent) components, we present limits to these interactions separately as is customary in the literature.

Limits on the scalar interactions, originally reported in [13], consider the WIMP coupling to protons and neutrons as identical, and therefore is given as the 'WIMP-nucleon' cross section. Normalizing the cross section to a single nucleon is done for two reasons. First, it facilitates accurate comparisons with other WIMP search experiments that use

different nuclei. Second, it removes all WIMP particle physics model dependence and thus does not rely on Supersymmetry, Kaluza-Klein, etc. for interpretation. The spin-indendent WIMP-nucleon cross section is shown in Fig 2.

Treatment of the spin-dependent cross section is in general more complicated than for the spin-independent case. It requires knowledge of the detailed nuclear structure of the two xenon odd isotopes, in particular, the spatial distribution of nucleons and distribution of nuclear spin between protons and neutrons. For $^{131}$Xe we follow the recommendation of [14] and use the shell model of [15]. For $^{129}$Xe there exist two leading shell models [16, 17], the former giving slightly better agreement between theory and measurement of the nuclear magnetic moment. Consequently, the two limits we report are based on 'main form factor' with the former and 'alternate form factor' with the latter. These limits were first reported in [18].

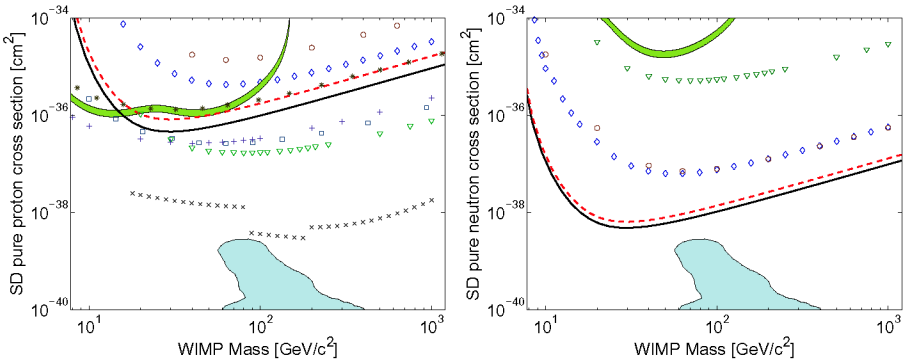


**FIGURE 3.** Upper limits on the spin-dependent WIMP cross section for (left) pure proton coupling and (right) pure neutron coupling with the (solid line) main form factor, and (dashed line) alternate form factor. Also shown are the results from the CDMS experiment [19] (diamonds), ZEPLIN-II [20] (circles), KIMS [21] (triangles), NAIAD [22] (squares), PICASSO [23] (stars), COUPP [24] (pluses), SuperK [25] (crosses), as well as the DAMA evidence region under the assumption of standard WIMP nuclear recoils and dark halo parameters (narrow green filled region) [26]. Favored regions from [10] are shown as the blue filled regions.

We present limits based on pure proton and pure neutron coupling separately, seen in Fig 3. As both of xenon's odd isotopes contain unpaired neutrons, our search is significantly more sensitive to the pure WIMP-neutron scattering cross section.

Some attention has been focused recently on the possibility that much of the dark matter could be in the form of a weakly interacting heavy Majorana neutrino, $\nu_M$. This particle arises in minimal technicolor theories [27, 28], and could have been produced in the early Universe under various dynamical dark energy models. The scattering cross section of $\nu_M$ is supressed relative to that of the heavy Dirac neutrino because *only* axial vector interactions are allowed for $\nu_M$. The $\nu_M$-nucleus scattering cross section in the limit of zero momentum transfer is given by [12, 29],

$$\sigma_{\nu_M} = \frac{8G_F^2}{\pi\hbar^4}\mu^2 I_s,$$

where $G_F$ is the Fermi constant, $\mu$ is the reduced mass, and $I_s$ is a factor that contains the nuclear spin structure and couplings. Form factors relating this to the cross section at non-zero momentum transfer are derived from the Xe nuclear shell models, and are the same form factors used in calculating the spin-dependent WIMP cross section limits. The background data shown in Fig 2 excludes at the 90% confidence level $\nu_M$ with mass between 9.4 GeV/$c^2$ - 2.2 TeV/$c^2$ (9.6 GeV/$c^2$ - 1.8 TeV/$c^2$ for the alternate form factor). We note that an analysis of LEP data has already excluded $\nu_M$ with mass below half the Z-boson mass (45.6 GeV/$c^2$) [30].

## REFERENCES


1. G. Jungman, M. Kamionkowski, K. Griest, *Phys. Rep.* **267**, 195 (1996)
2. G. Bertone, D. Hooper, J. Silk, *Phys. Rep.* **405**, 279 (2005)
3. R. J. Gaitskell, *Annu. Rev. Nucl. Part. Sci.* **54**, 315 (2004)
4. L. Baudis, *Int. J. Mod. Phys. A* **21**, 1925 (2006)
5. T. Doke, K. Masuda, E. Shibamura, *Nucl. Inst. and Meth. A* **291**, 617 (1990)
6. E. Aprile *et al*, *Phys. Rev. Lett.* **97**, 081302 (2006)
7. P. Sorensen *et al*, doi:10.1016/j.nima.2008.12.197 (to be published in Nucl. Instrum. Meth. A, Jan 2009)
8. Z. Ahmed *et al* (CDMS Collaboration), *Phys. Rev. Lett.* **102**, 011301 (2009)
9. J. Ellis, K. A. Olive, Y. Santoso, V. C. Spanos, *Phys. Rev. D* **71**, 095007 (2005)
10. L. Roszkowski, R. Ruiz de Austri, R. Trotta *J. High Energy Phys.* **07**, 075 (2007)
11. S. Yellin, *Phys. Rev. D* **66**, 032005 (2002)
12. J. D. Lewin, P.F. Smith, *Astropart. Phys.* **6**, 87 (1996)
13. J. Angle *et al* (XENON Collaboration), *Phys. Rev. Lett.* **100**, 021303 (2008)
14. M. T. Ressell and D. J. Dean, *Phys. Rev. C* **56**, 535 (1997)
15. J. Engel, *Phys. Rev. B* **264**, 114 (1991)
16. M. Hjorth-Jensen, T. T. S. Kuo, and E. Osnes, *Phys. Rep.* **261**, 125 (1995)
17. V. G. J. Stoks *et al*, *Phys. Rev. C* **49**, 2950 (1994)
18. J. Angle *et al* (XENON Collaboration), *Phys. Rev. Lett.* **101**, 091301 (2008)
19. D. S. Akerib *et al* (CDMS Collaboration), *Phys. Rev. D* **73**, 011102 (2006)
20. G. J. Alner *et al* (ZEPLIN-II Collaboration), *Phys. Lett. B* **653**, 161 (2007)
21. H. S. Lee *et al* (KIMS Collaboration), *Phys. Rev. Lett.* **99**, 091301 (2007)
22. G. J. Alner *et al* (UKDMC Collaboration), *Phys. Lett. B* **616**, 17 (2005)
23. M. Barnabe-Heider *et al* (PICASSO Collaboration), *Phys. Lett. B* **624**, 186 (2005)
24. E. Behnke *et al* (COUPP Collaboration), Science **319**, 933 (2008)
25. S. Desai *et al* (Super-Kamiokande Collaboration), *Phys. Rev. D* **70**, 083523 (2004)
26. C. Savage, P. Gondolo, and K. Freese, *Phys. Rev. D* **70**, 123513 (2004)
27. K. Kainulainen, K. Tuominen, and J. Virkajarvi, *Phys. Rev. D* **75**, 085003 (2007)
28. C. Kouvaris, *Phys. Rev. D* **76**, 015011 (2007)
29. J. Primack, D. Seckel, B. Sadoulet, *Ann. Rev. Nucl. Part. Sci.* **38**, 751 (1988)
30. S. Eidelman *et al* (Particle Data Group), *Phys. Lett. B* **592**, 1 (2004)